EARTH'S CRYOSPHERE
SCIENTIFIC JOURNAL

Earth`s Cryosphere, 2018, vol. XXII, No. 2, pp. 14–25 **http://earthcryosphere.ru/**

ICE AND FROZEN GROUND PROPERTIES

DOI: 10.21782/EC2541-9994-2018-2(14-25)

HOW AIR BUBBLES FORM IN POLAR ICE

V.Ya. Lipenkov

Arctic and Antarctic Research Institute, 38, Bering str., St. Petersburg, 199387, Russia; lipenkov@aari.ru

Experimental results for 22 ice cores from Antarctica and Greenland provide insights into principal mechanisms that govern the formation and evolution of air bubble systems in polar ice. A semi-empirical model has been suggested to relate the size and number of bubbles in ice with snow accumulation rate and temperature during ice formation. Air bubble sizes and specific numbers (number concentrations) can be used as reference for updating paleoclimate reconstructions based on ice core data.

Air bubble, polar ice formation, ice core, paleoclimate reconstruction

INTRODUCTION

Ice cores recovered from polar ice sheets store universal and reliable records of past climates and environments [*Petit et al., 1999*]. Most of paleoclimate reconstructions from ice core data use chemical analyses of ice and atmospheric air it has entrapped as inclusions (air bubbles). Isotope depth profiles of ice

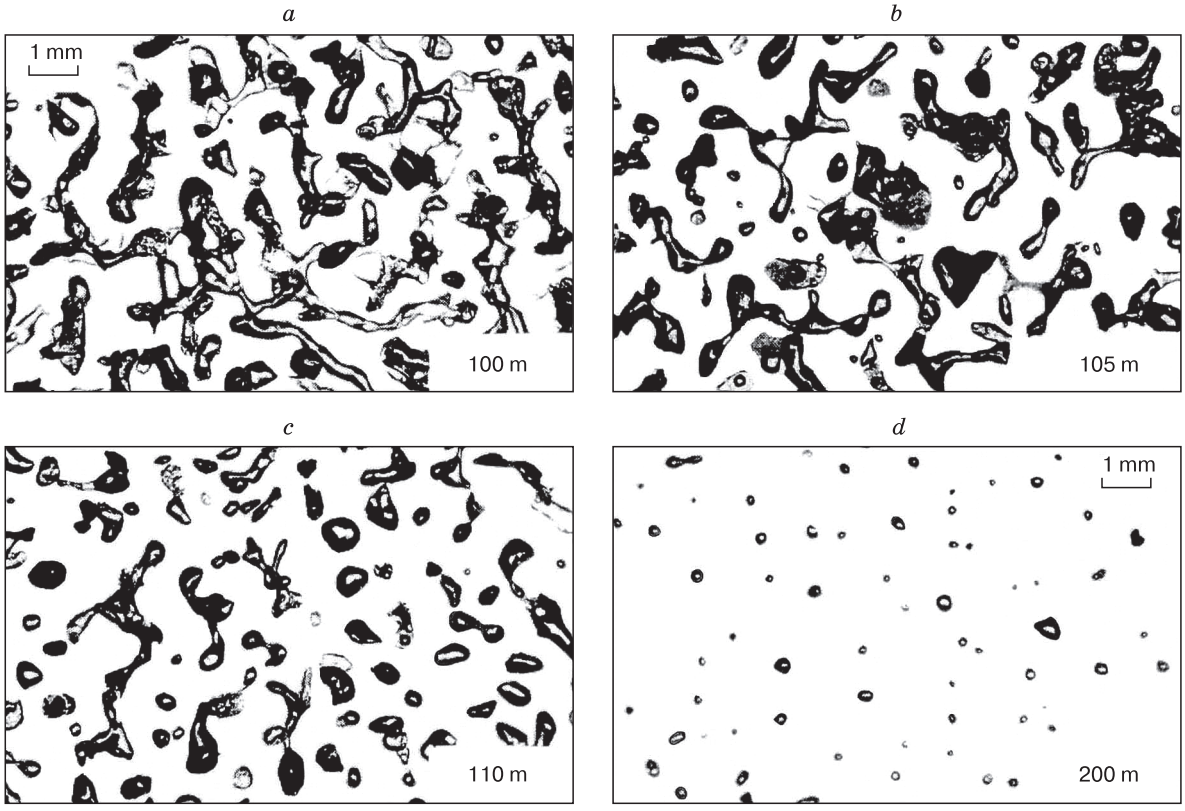

Fig. 1. Pores and air bubbles in Vostok ice core.

a: 100 m depth: close-off of firn pores and their isolation from atmospheric air, according to gas contents in ice; *b*: 105 m depth: close-off of firn pores, according to open porosity measurements; *c*: 110 m depth: disintegration of elongated air bubbles; *d*: 200 m depth: isometric air bubbles. Microbubbles occurr as nearly spherical small bubbles (*a*–*c*) or as black points (*d*).

cores have implications for past temperatures and snow accumulation rates in Antractica. However, the reconstructions made using isotope paleothermometers still bear large uncertainty and require additional checks [*Jouzel et al., 1997; Salamatin et al., 1998*].

Air bubbles entrapped during ice formation, and their geometrical parameters (Fig. 1), bear quantitative genetic information on recrystallized polar ice which can be used for independent assessment of past climatic conditions [*Lipenkov et al., 1998; Alley and Fitzpatrick, 1999*]. The first evidence for climate signals in measured depth profiles of air bubble parameters was obtained from ice cores recovered at the Russian station Vostok in Antarctica: their size and number were found out to correlate with hydrogen isotope composition (δD) of ice [*Barkov and Lipenkov, 1984*].

This study focuses on principles that govern the formation and evolution of air bubbles in polar ice on the basis of previous results [*Lipenkov et al., 1999; Lipenkov, 2000; Lipenkov and Salamatin, 2014*], with reference to recent advanced models of snow and firn densification [*Salamatin and Lipenkov, 2008; Salamatin et al., 2009*]. The new results make basis for an updated model relating the parameters of the air bubble-ice system with ice formation conditions. The model has been tested against a large set of experimental data, including those from ice cores recovered in different parts of Antarctica.

EXPERIMENTAL DATA

The size and number concentration or specific number of atmospheric gas inclusions (air bubbles) in ice are their main geometrical parameters. The specific number N (count per unit mass) is commonly quoted as the number of bubbles per 1 g of bubbly ice; the size of a single bubble is quoted as a radius r of a volume-equivalent sphere, while a cluster (an ensemble) of bubbles is characterized by the mean radius $\langle r \rangle$ and its standard deviation $\sigma(r)$, or the variance $s = \sigma(r) / \langle r \rangle$. Note that the variance s is, at the same time, the standard deviation of relative bubble radiuses and is only a few percent different from the lognormal standard deviation $\sigma(\ln r)$ in the case of lognormal size distribution. The two values are related as $\sigma^2(\ln r) = \ln (1 + s^2)$.

The sizes and specific numbers of air bubbles are commonly measured with a binocular microscope in 6 × 8 cm ice plates (thick sections), 2–3 mm thick, cut along the core axis. The classical method of manual counting was detailed in [*Lipenkov, 2000*]. Lately a new technique has come into use: automatic processing and analysis of digital photomicrographs of thick ice-core sections exhibiting bubble-like features [*Ueltzhöffer et al., 2010; Bendel et al., 2013*]. The first data thus obtained for ice cores from the Concordia and Kohnen research stations agree, within an experimental error, with the measurements by the author used in this study.

Figure 2 shows measured numbers of air bubbles from the Vostok [*Lipenkov and Salamatin, 2014*], Dome Fuji [*Ohno et al., 2004*], and Concordia (this study) ice cores. According to isotope analysis of ice, the depth profiles of air bubble properties presented in Fig. 2 span Holocene ice sheets that formed under conditions similar to the modern climate and during the Last Glacial maximum (LGM). Slow ice accumulation rates typical of the drilling area in Central Antarctica represent relatively shallow depths of LGM deposits. As a consequence, the zone where trapped air converts into clathrate hydrate lies below the ice deposited during the Last Glacial termination. Thus air bubbles in the LGM ice show a significant increase in number associated with cooling and deceleration of snow accumulation at that time (Fig. 2).

The model relating the geometrical parameters of air bubbles with climate parameters was calibrated using sizes and numbers of bubbles in Holocene ice in areas with different ice formation conditions. The study bases on original experimental results, as well as on published evidence available by the time being on the size and number of air bubbles in Antarctic and Greenland ice cores. The present ice formation conditions and parameters of air bubbles at 22 drill sites are summarized in Table 1.

NORMAL AIR BUBBLES AND MICROBUBBLES

Atmospheric air makes up about 10 vol.% of young polar ice. Most of air becomes entrapped when firn pores close off and forms gas inclusions classified as hypogenic by *Shumskiy* [*1955*]. In polar ice sheets, the process completes at depths from 60 to 125 m, depending on ice formation conditions. The age of ice at these depths, counted from the time when solid precipitation was deposited upon the ice sheet surface, may vary from a few tens to a few thousands of years (Table 1). Additionally, polar ice contains numerous very small air bubbles (microbubbles) captured by ice grains during their growth in snow or firn, long before the complete isolation of firn pores from the atmosphere [*Lipenkov, 2000*]. According to the classification of *Shumskiy* [*1955*], microbubbles are authigenic inclusions. They are easily spotted in the upper part of ice sheets due to their location inside ice grains, small sizes, and round shapes (Fig. 1).

The existence of two generations of air inclusions is confirmed by an experimentally observed bimodal size distribution (Fig. 3, *a*), as well as by direct measurements of gas pressure inside bubbles. The latter measurements show that gas pressure in normal bubbles (hypogenic inclusions) at the firn/ice transition is, on average, 0.6 MPa lower than the overburden ice pressure, while the average pressure difference

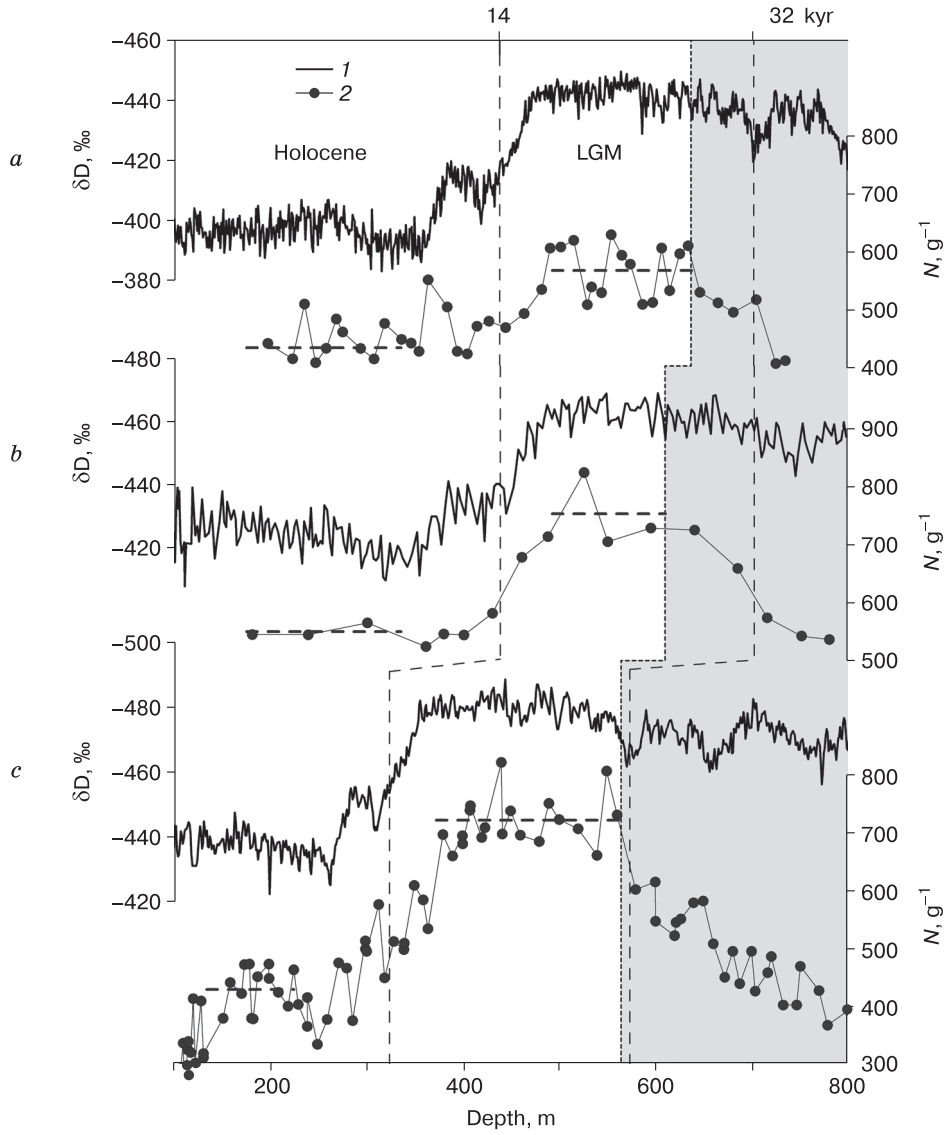

Fig. 2. Depth-dependent variations of hydrogen isotope composition (δD) and specific number of air bubbles (*N*) in Antarctic ice cores from stations Concordia (*a*), Dome Fuji (*b*) and Vostok (*c*).

1 – δD (‰) according to different estimates: [*Jouzel et al., 2007*] (*a*), [*Watanabe et al., 2003*] (*b*), [*Petit et al., 1999*] (*c*) (δD scales are inverse); *2* – number of air bubbles per unit mass (*N*, g^{-1}), according to different estimates: this study (*a*), [*Ohno et al., 2004*] (*b*), [*Lipenkov and Salamatin, 2014*] (*c*). Horizontal dash lines are average *N* in LGM ice deposited in Holocene climate. Shaded area is zone of ice-to-clathrate conversion. Vertical dash lines delineate ice layers corresponding to the ages 14 kyr (middle of the LGM–Holocene boundary) and 32 kyr (onset of LGM according to isotope data).

in microbubbles (authigenic inclusions) is 0.25 MPa [*Lipenkov, 2000*].

Studies of Antarctic ice cores from different areas show that microbubbles make up commonly (20 ± 5) % of the total population of air bubbles. Meanwhile, their contribution into the total gas content and porosity of ice does not exceed 0.3 %, and, hence, their impact on ice densification and composition of entrapped air is vanishing. Therefore, the consideration below is restricted to normal bubbles.

CORRELATION OF SIZES AND NUMBERS OF AIR BUBBLES WITH ICE MICROSTRUCTURE AT THE FIRN/ICE TRANSITION

Pores of firn that has reached a relative density of 0.8 look like cylindrical channels (Fig. 4, *a*) along the edges of ice crystals similar in shape to equilibrium polyhedrons that fill the whole space, like tetrakaidecahedrons of Lord Kelvin and Robert Williams [*Maeno and Ebinuma, 1983*]. Pores in firn close off and the air remaining in the pore volume becomes

Table 1. **Present ice formation conditions and parameters of air bubbles in Holocene ice at 22 drill sites in Antarctica and Greenland**

No.	Drill site	Coordinates	T, °C	b, g/(cm^2·yr)	d_s	τ_c^*	τ_c	A_c, mm^2	$\langle r_c \rangle$, mm	s	N, g^{-1}	Error N (±g^{-1})	Reference
						years							
1	Dai 3	65°11′ N, 43°49′ W	−20.0	50.0	0.39	–	81	2.26	0.42		300	60	[*Shoji and Langway, 1985*]
2	KM60	67°05′ S, 93°19′ E	−20.8	46.3	0.46	78	88	2.26			360	31	[*Lipenkov et al., 1999*]
3	KM73	67°12′ S, 93°17′ E	−21.1	50.0	0.45	90	83	2.16			355	41	[*Lipenkov et al., 1999*]
4	KM105	67°26′ S, 93°23′ E	−24.5	31.4	0.46	131	130	2.32			450	27	[*Lipenkov et al., 1999*]
5	Berkner	78°36′ S, 45°43′ W	−26.0	13.0	0.43	238	268	3.49			239	20	*This study*
6	KM140	67°45′ S, 93°39′ E	−27.0	40.4	0.48	121	114	1.86	0.40	0.35	345	42	[*Lipenkov et al., 1999*]
7	Siple Dome	81°65′ S, 148°81′ E	−27.0	10.0	0.42	293	338	3.87			232		*This study*
8	Berd	80°00′ S, 120°00′ W	−28.7	16.0	0.41	251	245	2.70	0.43		250	40	[*Gow and Williamson, 1975*]
9	KM200	68°15′ S, 94°05′ E	−30.5	26.4	0.49	175	174	1.93			360	65	[*Lipenkov et al., 1999*]
10	WAIS	79°28′ S, 112°05′ W	−31.0	20.2	0.42	–	217	2.14			400	15	[*Fegyveresi et al., 2011*]
11	NGRIP	75°06′ N, 42°19′ W	−31.5	17.5	0.35	–	272	2.40			335	20	[*Kipfstuhl et al., 2001*]
12	GRIP	72°35′ N, 37°38′ W	−31.7	21.2	0.41	220	224	2.09			290	50	[*Pauer et al., 1999*]
13	KM260	68°46′ S, 94°28′ E	−33.5	6.9	0.51	455	535	3.39	0.41	0.37	270	52	[*Lipenkov et al., 1999*]
14	KM325	69°18′ S, 95°01′ E	−37.0	14.0	0.49	356	339	1.91	0.38	0.35	380	45	[*Lipenkov et al., 1999*]
15	KM400	69°57′ S, 95°37′ E	−39.9	15.4	0.47	389	342	1.59	0.36	0.33	485	49	[*Lipenkov et al., 1999*]
16	Talos Dome	72°49′ S, 159°11′ E	−41.0	8.0	0.40	637	650	2.21			306	33	*This study*
17	Kohnen	75°00′ S, 00°04′ E	−44.6	6.4	0.37	877	859	2.03			368	49	*This study*
18	Komsomol-skaya	74°06′ S, 97°30′ E	−53.8	6.4	0.36	1256	1141	1.22	0.30	0.38	650	16	[*Lipenkov et al., 1999*]
19	Concordia	75°06′ S, 123°21′ E	−54.5	2.5	0.36	2508	2425	1.86			432	19	*This study*
	Concordia (LGM)							1.37			565	20	*This study*
20	Vostok	78°28′ S, 106°48′ E	−57.0	2.1	0.35	3054	3014	1.74	0.33	0.43	430	19	[*Lipenkov and Salamatin, 2014*]
	Vostok (LGM)							1.12	0.28	0.37	723	20	[*Lipenkov, 2000*]
21	Dome Fuji	77°19′ S, 39°42′ E	−57.3	3.1	0.34	2424	2249	1.39			551	20	[*Ohno et al., 2004*]
	Dome Fuji (LGM)							1.08			754	60	[*Ohno et al., 2004*]
22	Dome A	80°22′ S, 77°22′ E	−58.5	2.32	0.41		2933	1.50			567	75	*This study*

Note. T is snow temperature at the depth where it becomes seasonally invariable (10–15 m); b is snow accumulation rate; d_s is relative density of snow on ice sheet surface; τ_c^* and τ_c are, respectively, ages of ice at the firn/ice transition, measured and calculated using equation (11); A_c is calculated ice grain size at the firn/ice transition; $\langle r_c \rangle$ and s are, respectively, mean radius of air bubbles at the firn/ice transition and its variance; N is measured number of air bubbles per unit mass, with two-sigma error. N and A_c values for LGM ice are additionally quoted for Vostok, Concordia and Dome Fuji cores (Fig. 2).

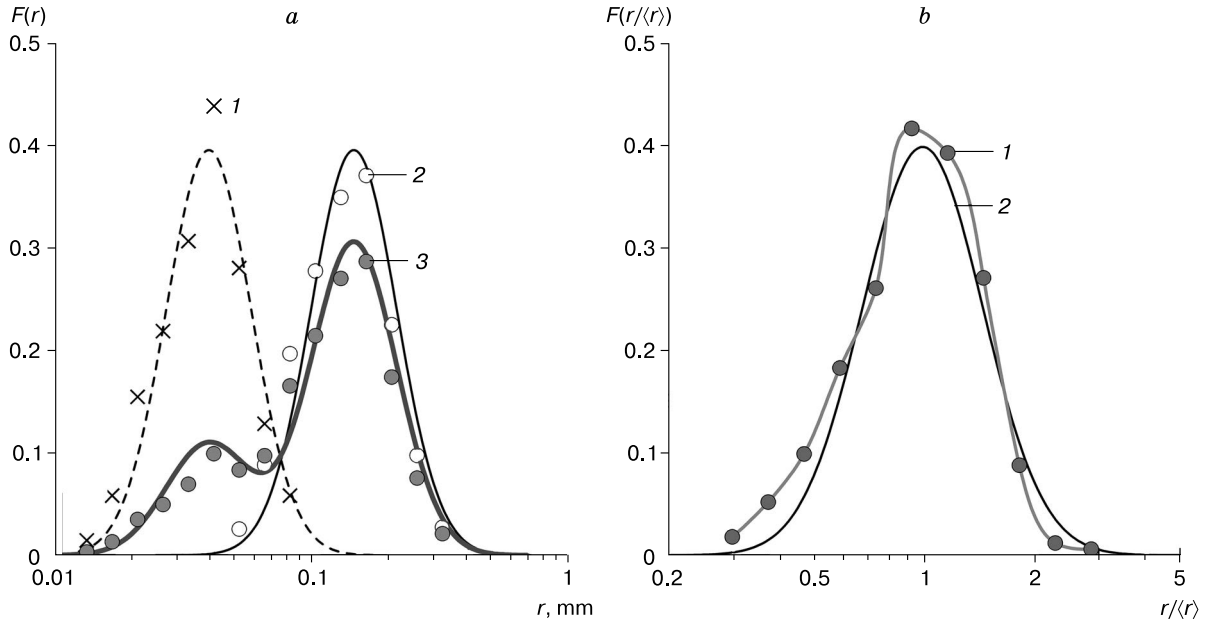

Fig. 3. Size distribution of air bubbles in polar ice.

a: normalized distributions $F(r)$ of microbubbles (*1*), normal bubbles (*2*) and all air bubbles (*3*) from their radiuses in Vostok ice core recovered from the depth 183 m (measurements of 2500 inclusions); symbols are measured data; curves are lognormal size distributions corresponding to measured data and bimodal distribution on their basis, for all inclusions; *b*: self-similar size distribution of normal air bubbles $F(r/\langle r\rangle)$, estimated from measurements of 11 000 inclusions at different depths at six drill sites (*1*) and the respective lognormal size distribution (*2*).
Normalized probability density function: $F(x) = dN/(NdX)$, where $X = (\ln x - \langle \ln x \rangle)/\sigma(\ln x)$; x is radius r (*a*) or relative radius $r/\langle r \rangle$ (*b*) of air bubbles. Lognormal distribution is defined by equation $F(x) = (2\pi)^{-0.5} \exp(-X^2/2)$.

enclosed in isolated bubbles within a relatively thin ice sheet layer where the relative firn density ranges from 0.85 to 0.93 [*Stauffer et al., 1985*]. Ice at this depth consists of aggregates of uniformly sized polyhedrons (ice grains) with cylindrical channels (elongated pores) along their edges (Fig. 4, *b*). The total length of the channels per unit mass (L) is related with the length of the polyhedron edges (l) as

$$L = y \Big/ \left(\rho_i \varphi_v l^2\right), \qquad (1)$$

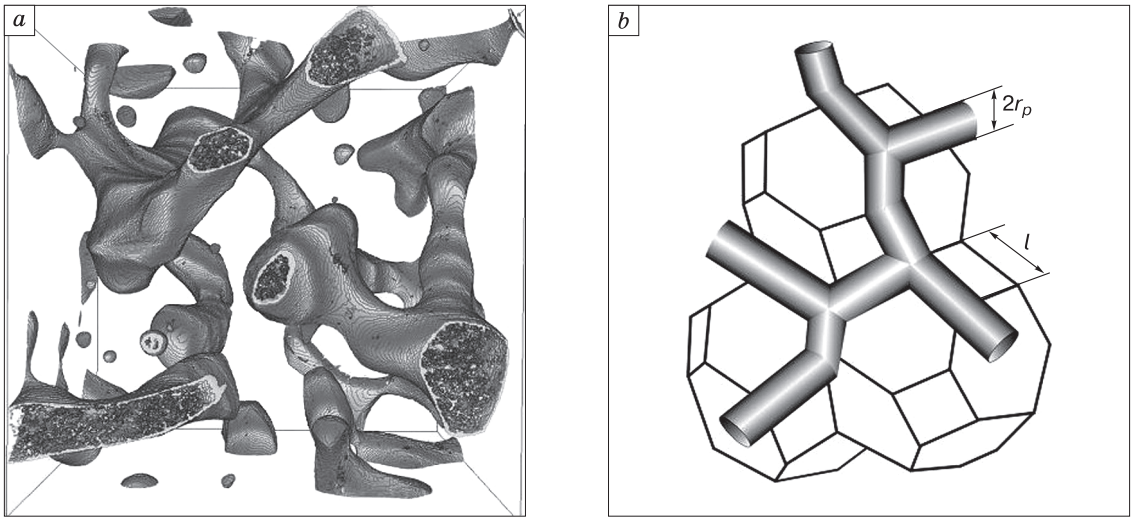

Fig. 4. X-ray tomographic 3D image of firn pores (*Barnol, personal communication*) (*a*) and sketch of ice microstructure at the firn/ice transition (*b*).

r_p is pore radius; l is length of polyhedron edge.

where y is the number of edges per grain; ρ_i is the pure ice density; φ_v is the constant relating the polyhedron volume ($\varphi_v l^3$) with the edge length [*Underwood, 1970*].

The porosity c of an ice aggregate is related with the pore radius r_p and the total length L as

$$c/(1-c) = \pi r_p^2 L \rho_i . \quad (2)$$

The elongated pores with a nonzero Gibbs surface free energy are known [*Nichols and Mullins, 1965*] to be unstable and pinched off to form closed spherical pores because of the surface curvature gradient. This gradient leads to redeposition of material on the walls of cylindrical pores in ice, necking, and eventually to breakdown of the pores. The necks (perturbations) on the pore walls grow the fastest at different ratios $\alpha = \lambda/r_p$ (where λ is the perturbation wavelength) depending on the mass transfer mechanism, but the growth rates are always positive at $\alpha > 2\pi$. If necking occurs by the vapor transport mechanism, as expected for pinched-off firn pores [*Maeno and Ebinuma, 1983*; *Alley and Fitzpatrick, 1999*], its rates are the highest at $\alpha \approx 9$, provided that they are controlled by the mass transfer rates [*Shieh and Evans, 1991*].

The level where the pores close off completely and the pore air becomes isolated from atmospheric air in terms of pressure is assumed to be the firn/ice transition. Correspondingly, this interface lies at the depth (let it be h_c) where the measured density of ice equals its gas content normalized to the ice temperature and atmospheric pressure [*Martinerie et al., 1992*].

Further evolution of air bubble systems below h_c consists in disintegration of elongated bubbles and relaxation compression of all air inclusions under the pressure lag Δp between the ice matrix and the entrapped air. By definition, the disintegration of inclusions does not change their total volumetric content but increases the number of air bubbles in ice. The process continues until the length/radius ratio of all bubbles reduces to 2π. In the Vostok cores, this condition fulfills at a depth of 160–170 m (i.e., 60–70 m below the firn/ice transition). At the same time, isometric inclusions make up about 50 % of the total bubble population already at the depth 105 m and about 80 % at 110 m, while the length/radius ratio for elongated inclusions at the 110 m level rarely exceeds 4π (Fig. 1). Thus, disintegration of normal bubbles in ice mainly completes, and their number becomes constant, within first ten meters below h_c. Note that the mean radius of elongated inclusions within this narrow depth interval is only a few percent smaller than the pore radius r_{pc} at the firn/ice transition (see below).

According to the above, the final specific number N of isometric bubbles in ice is approximately [*Lipenkov et al., 1999*]

$$N = L_c / (\alpha r_{pc}), \quad (3)$$

where α is a constant. Herebelow the subscript c refers to values of the respective parameters at the firn/ice transition.

In the glaciological practice, ice grain sizes are most often estimated via average cross section areas (A) measured in ice thin sections. In a system of equigranular polyhedrons assumed here to approximate the firn microstructure at the depth h_c, this area is

$$A = \varphi_A l^2,$$

where φ_A is the geometric coefficient defined by the polyhedron type [*Underwood, 1970*]. With this assumption, and with equations (1)–(3), the geometrical parameters of air bubbles are:

$$N = G / A_c^{1.5}, \quad G = \frac{\sqrt{\pi}}{\alpha \rho_i} \left(y \frac{\varphi_A}{\varphi_v} \right)^{1.5} \left(\frac{1-c_c}{c_c} \right)^{0.5}, \quad (4)$$

where α is a constant ($\alpha > 2\pi$) that refers to average size and number of spherical inclusions at the given porosity c_c and the grain size A_c at the firn/ice transition.

In the first approximation, the pure ice density and the ice porosity at the firn/ice transition can be assumed constant ($\rho_i = (0.922 \pm 0.003)$ g/cm^3, $c_c = 0.10 \pm 0.01$) in the considered temperature range. Correspondingly, the complex coefficient G in (4) is constant as well, being a more rigorous formulation of the statement [*Gow, 1968*] that the number and size of air bubbles in ice mainly depend on the size of ice grains at the firn/ice transition.

Theoretical [*Shreve, 1967*] and experimental [*Stehle, 1967*] studies of the migration of air bubbles in ice under a temperature gradient show that the process cannot change significantly the initial number of gas inclusions in polar ice. In the absence of considerable deformation of polar ice, neither coalescence of air bubbles [*Weertman, 1968*] nor their disintegration as a result of uneven deformation in neighbor ice grains [*Alley and Fitzpatrick, 1999*] can influence much the number N. Air bubbles are unlikely to coalesce while ice grains are growing because they are small and move rapidly away from migrating grain boundaries below the firn/ice transition [*Gow, 1969*]. Thus, there are all reasons to expect that the number of air bubbles in polar ice remains invariable after their disintegration has completed at the depth $h = h_d$, till the depth where the entrapped air converts to clathrate hydrate ($h = h_{trans}$). A system of air bubbles in sinking layers of polar ice at the depths $h_d < h < h_{trans}$ can change its geometrical parameters uniquely by compression of bubbles under the overburden ice pressure.

SIZE DISTRIBUTION OF AIR BUBBLES AFTER THEIR DISINTEGRATION

Unlike the simplified model presented in Fig. 4, *b*, the sizes of real ice grains and pore radiuses at the firn/ice transition are highly variable

(Fig. 4, *a*). Correspondingly, an ensemble of air bubbles that forms below the firn/ice transition is a heterogeneous system in terms of grain sizes and internal gas pressure. The evolution of such a system within the depths $h_d < h < h_{trans}$ can be analyzed theoretically using the model of bubbly ice densification [*Lipenkov et al., 1997; Salamatin et al., 1997*] formulated for a system of uniformly sized air bubbles. In this case the model is applied to simulate relaxation compression of air bubbles that belong to different size groups. As shown by previous studies [*Lipenkov and Salamatin, 2014*], (i) the shape of bubble size distribution remains time-invariant after disintegration during compression, i.e., the variance of bubble radiuses at any depth equals that at the depth of complete disintegration: $s = s_d$ = const; (ii) ensembles of air bubbles that arise under different conditions of polar ice formation have the same self-similar size distribution approaching the lognormal distribution with $\sigma(\ln r) = 0.37 \pm 0.05$, $s = 0.38 \pm 0.05$ (Fig. 3, *b*).

However, the pore close-off depth h_c is more suitable than h_d for comparing air bubble systems in different ice formation conditions, because their geometrical parameters at this depth (at the firn/ice transition) are independent of internal air pressure but depend only on ice grain size (see equation (4)).

The air bubble sizes at h_c are considered for an ideal system of spherical bubbles which would exist at this depth if they all disintegrated instantaneously and simultaneously with pore isolation, rather than for a complex system of elongated and often branching gas inclusions occurring in reality at h_c (Fig. 1, *a*).

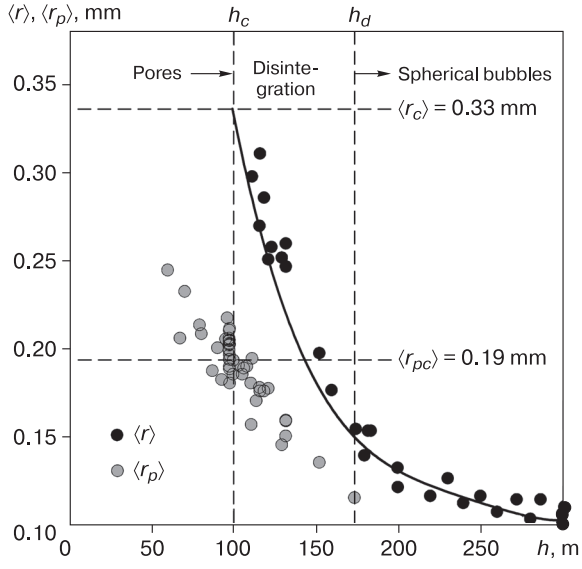

Fig. 5. Depth-dependent variations of mean equivalent radius of air bubbles $\langle r \rangle$ and mean radius of cylindrical pores and air bubbles $\langle r_p \rangle$ in the upper ice sheet part at the Vostok station.

Circles are measured data; curve is calculated $\langle r \rangle(h)$ depth profile for initial radius $\langle r_c \rangle$ = 0.33 mm typical of Holocene climate (see text for explanation).

The ideal system is equivalent in volume to the real system, and the air bubbles have the same volumetric content but their number and relative size distribution correspond to those in fully disintegrated inclusions. In steady-state climate conditions, the distribution of abstract spherical bubbles at the firn/ice transition $F_c(r_c)$ is related to the distribution of real bubbles $F(r)$ at any depth within the $h_d < h < h_{trans}$ interval as [*Lipenkov and Salamatin, 2014*]

$$F_c(r_c) = F(r_c/\zeta)/\zeta, \quad \zeta = \frac{r_c}{r} = \left(\frac{pT_c}{Tp_c}\right)^{1/3}, \qquad (5)$$

where r, T, p are, respectively, the bubble radius, temperature, and average air pressure at the depth $h_d < h < h_{trans}$; r_c, T_c, p_c are the respective parameters of the system at the firn/ice transition prior to compression of bubbles. The pressure p is calculated from the model of bubbly ice densification [*Salamatin et al., 1997*]. The variance of bubble sizes at the pore close-off depth is $s_c = s$, while the mean bubble radius $\langle r_c \rangle$ is

$$\langle r_c \rangle = \zeta \langle r \rangle. \qquad (6)$$

These equations, along with measured bubble sizes at different depths from eight drill sites, were used to estimate $\langle r_c \rangle$ and s_c typical of different polar ice formation conditions during the present climate stage (Table 1). The existence of lognormal self-similar size distribution of air bubbles means that $\langle r_c \rangle$, s and N in Table 1 represent the geometrical parameters of air bubbles controlled by their relation with ice grain sizes at the firn/ice transition. The relative volume of lognormally distributed air bubbles (ice porosity c) is given by [*Saltykov, 1976*]:

$$c/(1-c) = (4/3)\pi \langle r \rangle^3 k^3 N \rho_i,$$

$$k = \exp\left(\sigma^2(\ln r)\right) = 1 + s^2. \qquad (7)$$

In perfect accordance with (7), the available data on sizes and numbers of air bubbles in ice (Table 1) demonstrate a distinct linear correlation ($R^2 = 0.94$) between the values of $1/\langle r_c \rangle^3$ obtained independently in experiments and N. Errors in $\langle r_c \rangle$ inferred from known N using the constant $s = 0.38$ do not exceed 3 %, and errors in N inferred from $\langle r_c \rangle$ are within 10 % [*Lipenkov and Salamatin, 2014*].

The steady-state Holocene depth profile of mean bubble radius $\langle r \rangle$ in the vicinity of the Vostok station (Fig. 5) calculated using (6) for the initial bubble size $\langle r_c \rangle$ = 0.33 mm deviates systematically from the measured values (black circles) only at the depths of bubble disintegration (99–170 m). The deviation is minor, which supports the inference that the disintegra-

tion of bubbles mainly completes within a few meters below the firn/ice transition (99–110 m). The measured radiuses of pores and cylindrical inclusions $\langle r_p \rangle$ (white circles in Fig. 5) are always smaller than the mean equivalent radius of bubbles $\langle r \rangle$. However, $\langle r_p \rangle$ decreases with depth more slowly than $\langle r \rangle$, i.e., most of cylindrical inclusions with a large radius survive disintegration.

Assuming instantaneous disintegration of all pores at the firn/ice transition, with the mean radius of pores and air bubbles at this depth being $\langle r_{pc} \rangle = 0.19$ mm and $\langle r_c \rangle = 0.33$ mm, the parameter α for air bubbles from the Vostok ice core can be estimated as

$$\alpha = \frac{4}{3}\left(\frac{\langle r_c \rangle}{\langle r_{pc} \rangle} \right)^3 \approx 7.$$

Independent calculations using equations (2) and (3) and measured N give $\alpha \approx 11.5$. The arithmetic mean of these two values, 9.2 ($\approx 2.9\pi$), is the most reliable empirical estimate of α, about $\alpha \approx 9$ obtained for the case of pore close-off mainly by the vapor diffusion mechanism [*Shieh and Evans, 1991*]. Generally, the above experimental results prove valid the suggested model explaining the formation of an ensemble of air bubbles in polar ice.

CLIMATE IMPACT ON GEOMETRICAL PARAMETERS OF AIR BUBBLE SYSTEMS

The growth of ice grains in firn is most often assumed (see the overview of *Thorsteinsson* [*1996*] and references therein) to follow the parabolic law meaning that the average cross section area of ice grains A increases linearly with the age of ice τ. Correspondingly, the size of ice grains at the firn/ice transition (A_c) is linearly related with their initial size on the ice sheet surface (A_s), growth rate (k), and total duration of the ice formation process (τ_c) as

$$A_c = A_s + k\tau_c. \qquad (8)$$

The empirical growth rates of ice grains (k) strongly correlate with firn temperatures according to the classical Arrhenius equation for thermally-induced processes:

$$k = k_0 \exp(-Q/RT), \qquad (9)$$

where Q is the activation energy of self-diffusion through grain boundaries in an ice aggregate; R is the universal gas constant; k_0 is the pre-exponential factor; T is the temperature during ice grain growth, K. In this study, Q and k_0 values are assumed to be $Q = 46$ kJ/mol and $k_0 = 4.2 \cdot 10^7$ mm^2/yr, as obtained for the temperature range from –57 to –20 °C from data on Antarctic and Greenland ice cores recovered at 18 drill sites [*Lipenkov et al., 1999*]. The same data indicate weak dependence of A_s [mm^2] on ice surface temperature (T_s, K), which satisfies the empirical equation

$$A_s = -1.83 + 1.08 \cdot 10^{-2} T_s. \qquad (10)$$

At steady-state climate conditions $T_s \approx T_c \approx T$, equations (8)–(10) allow estimating ice grain sizes at the firn/ice transition from the known age of ice at this depth and snow-firn temperature.

The time required for snow-to-ice conversion (age of ice at the firn/ice transition, τ_c) mainly depends on the temperature of the snow-firn pack (T) and the snow accumulation rate (b). A simple equation for calculating τ_c at the steady-state conditions of polar ice formation was derived by *Salamatin and Lipenkov* [*2008*] based on similarity analysis of ice density profiles using a physical model of snow-firn densification [*Salamatin et al., 2009*]:

$$\tau_c = B\left[\frac{\mu d^n}{(g\rho_i b)^n} \right]^{1/(1+n)}, \qquad (11)$$

$$\mu = \mu^* \exp\left[\frac{Q_p}{R}\left(\frac{1}{T} - \frac{1}{T^*} \right) \right],$$

where d is the average relative snow-firn density ($d = \rho/\rho_i$) between the ice sheet surface and the depth h_c; g is the gravitational acceleration; B is the dimensionless shape factor of the density-depth profile; $Q_p \approx 58$ kJ/mol is the activation energy of dislocation creep, and $\mu^* \approx 21$ MPa^n·yr is the temperature-dependent coefficient of nonlinear ice viscosity at $T^* \approx 215.7$ K for the creep exponent $n = 3.5$.

The model parameters d and B were determined in [*Salamatin et al., 2009*] for two types of ice sheet surface conditions: 1) $d = 0.709$, $B = 2.76$ at $T_s < -24$ °C and $d_s < 0{,}42$; 2) $d = 0.745$, $B = 2.40$ at $T_s > -40$ °C and $d_s > 0.38$; for the overlap range, average parameter values were applied.

The values τ_c and A_c calculated with (8)–(11) for the ice formation conditions (T, b, d_s) at 22 drill sites are listed in Table 1. Note that τ_c are slightly (3 % on average) underestimated relative to experimental data (τ_c^*), apparently due to possible systematic error in mean secular T and b values from current observations. Note also that the size of ice grains A_c (Table 1) was calculated for cubic-octahedral shape approximation, which was assumed [*Lipenkov et al., 1999*] for bringing together experimental data from different sources and is used for calculating Q and k in this study.

The $N\left(1/A_c^{1.5}\right)$ curve in Fig. 6, *a*, plotted using calculated A_c [mm^2] and measured N [g^{-1}] (Table 1) is a linear relationship, which is consistent with that between the number of air bubbles and the ice grain size at the firn/ice transition approximated as (4) with the constant G. Linear regression coefficients were calculated without data from drill site KM105,

which is located within the zone of gravity winds where the surface snow density is anomalously high for an area of cold polar ice formation. Least mean square calculations from 21 pairs of A_c [mm^2] and N [g^{-1}], exclusive of data from site KM105, give

$$N = 123 + 709 / A_c^{1.5}, \quad R^2 = 0.92. \qquad (12)$$

Equations (7)–(12) make up a semi-empirical model relating the specific number of air bubbles N and the mean air bubble radius at the firn/ice transition $\langle r_c \rangle$ with the ice formation conditions (T, b, d_s).

Note that average N values for air bubbles formed during the last glacial maximum (white diamonds in Fig. 6, *a*) obtained form the Vostok, Dome Fuji, and Concordia ice cores only slightly transcend the N range for bubbles in Holocene ice. Given that the LGM climate in central Antarctica was the coldest over at least past 800 kyr of the Earth's history [*Jouzel et al., 2007*], the calibration coefficients in (12) are valid for the whole range of polar ice formation conditions during the LGM event.

Model (8)–(12) was used to calculate a template for estimating the specific number of air bubbles in polar ice from snow temperature and accumulation rate corresponding to ice formation (Fig. 6, *b*), assuming constant density of surface snow, $d_s = 0.4$. The error in N estimated from known T and b corresponds to a random two-sigma error of $2\sigma \approx \pm 80$ g^{-1} (width of the shaded strip in Fig. 6, *a*).

Average specific numbers of air bubbles in LGM ice measured in the Concordia (565 g^{-1}), Dome Fuji (754 g^{-1}) and Vostok (723 g^{-1}) ice cores were used to calculate, with (8)–(12), the respective combinations of b and T at which ice could form at that time. The resulting $b(T)$ curves are compared in Fig. 7 with paleoclimate reconstructions for the LGM event obtained by the classical method, through interpretation of ice core isotope data, alone (A1–A4) and jointly with borehole temperature logs (B1–B3).

The standard practice of reconstructing past temperature variations on the Antarctic ice sheet surface refers to the present relation between the heavy hydrogen isotope composition (δD) of the deposited snow and temperature. In East Antarctica, the temperature dependence of δD in snow is linear, with a slope of $\Delta(\delta D)/\Delta T \approx 6$ ‰/°C, according to numerous route survey results. The applicability of this relationship to past temperature variations reconstructed form ice core isotope data is confirmed by calculations on the basis of isotope models of global atmospheric circulation [*Jouzel et al., 1997*]. Variations in past snow accumulation rates are estimated using temperature dependence of precipitation in Antarctica [*Robin, 1977*].

Independent evidence of past ice surface temperatures comes from temperature logs of deep boreholes, which are interpreted using models of heat and mass transfer in ice sheets with input data including

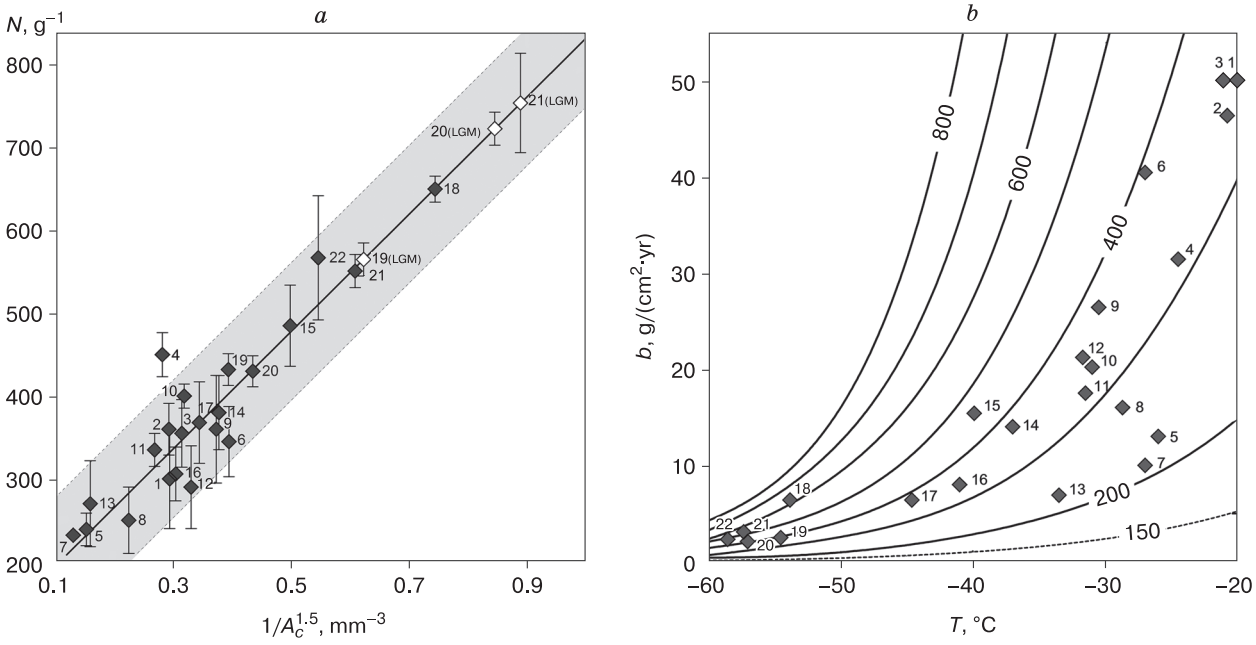

Fig. 6. Correlation between number of air bubbles in ice and conditions of polar ice formation.

a: specific number N of air bubbles vs. ice grain size at the firn/ice transition (A_c); vertical bars are 2σ errors in measured N (Table 1); shaded zone along regression line is zone of uncertainty (2σ) in N estimated from A_c; *b*: template relationship of N vs. snow temperature (T) and accumulation rate (b) during ice formation, calculated using model (8)–(12). 1–22 are numbers of drill sites (Table 1).

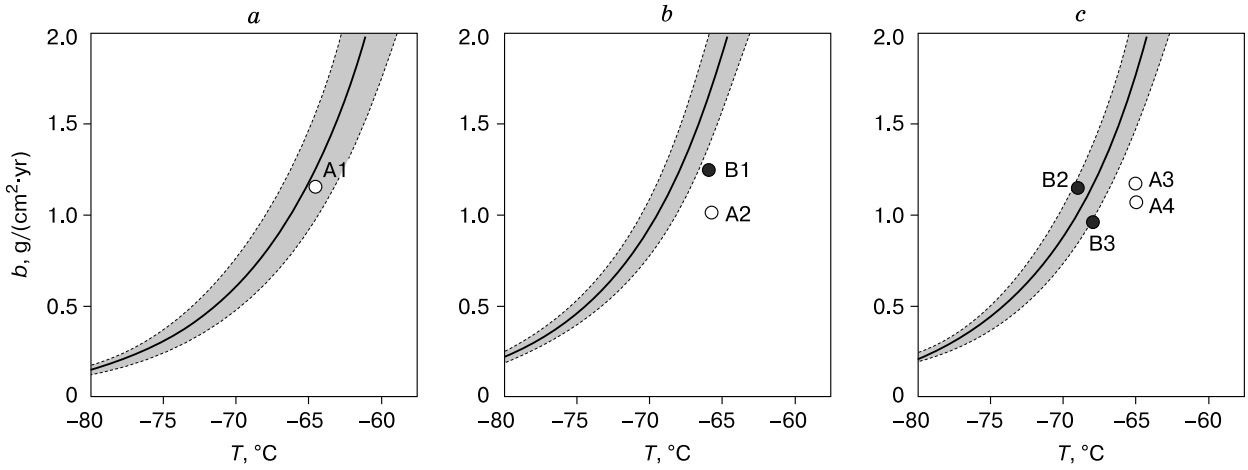

Fig. 7. Correlation between number of air bubbles in ice and reconstructed ice temperature T and accumulation rate b during Last Glacial Maximum at Concordia (a), Dome Fuji (b) and Vostok (c) stations.

Line is temperature dependence of ice accumulation rate corresponding to average specific number of air bubbles in LGM ice (Fig. 2; Table 1); shaded zone is 2σ error interval. White circles are T and b values reconstructed using classical approach to isotope data interpretation, according to different references: A1 [*Jouzel et al., 2007*], A2 [*Kawamura et al., 2007*], A3 [*Petit et al., 1999*], A4 [*Parrenin et al., 2004*]. Black circles are T and b reconstructed using isotope data and temperature logs, according to different references: B1 [*Hondoh et al., 2002*], B2 [*Salamatin et al., 1998*], B3 [*Tsyganova and Salamatin, 2004*].

temperature and accumulation rate series based on δD depth profiles. The temperature calibration of the isotope paleothemometer and the paleoreconstructions are updated by minimization of misfit between calculated and measured ice-sheet temperature profiles [*Salamatin et al., 1998*].

As follows from Fig. 7, the climate reconstructions from jointly interpreted δD and temperature logs are more reliable than those based on mere isotope data, and better agree with the estimated specific numbers of air bubbles in LGM ice. Thus, size and number of entrapped air bubbles, as structural and genetic proxies, provide good independent checks for paleoclimate reconstructions from ice core records.

CONCLUSIONS

The reported research has yielded a wealth of new experimental evidence on the number of air bubbles entrapped in ice cores from six areas in Antarctica with different climate conditions. The results reveal general principles that govern the formation of a system of air bubbles in polar ice and make basis for a semi-empirical model relating the size and specific number of bubbles with temperature and snow accumulation rate during ice formation. The derived equations have been carefully checked and calibrated against new and published data on the geometrical parameters of air bubbles from 22 ice coring sites in Antarctica and Greenland.

The results provide a theoretical background for a new method of paleoclimate reconstructions proceeding from correlation between the number and size of air bubbles in polar ice cores and ice formation conditions. Specifically, it is reasonable to use experimental depth profiles of the specific number of air bubbles, jointly with paleotemperature series inferred from ice core δD profiles and temperature logs of boreholes, for reconstructing past snow accumulation rates.

I wish to thank Professor A.N. Salamatin for insightful discussions and valuable advice during manuscript preparation.

The study was supported by grant 14-27-00030 from the Russian Science Foundation. Some theoretical postulates explaining formation and evolution of air bubbles in ice (time-invariant size distribution of air bubbles at steady-state climate conditions of ice formation) were obtained under a support of the Russian Foundation for Basic research (grant 06-05-65174). Ice core samples from the Concordia, Kohnen, Talos Dome, Siple Dome, and Dome A stations in Antarctica were provided as part of Russian-French collaboration (Laboratoire International Associé (LIA) "Climats et Environnements à Partir des Archives Glaciaires VOSTOK").

References

Alley, R.B., Fitzpatrick, J.J., 1999. Conditions for bubble elongation in cold ice–sheet ice. J. Glaciol. 45 (149), 147–153.

Barkov, N.I., Lipenkov, V.Ya., 1984. Quantitative characterization of ice structure at Vostok station to a depth of 1400 m. Materialy Glaciol. Issled. 51, 178–186.

Bendel, V., Ueltzhöffer, K.J., Freitag, J., Kipfstuhl, S., Kuhs, W.F., Garbe, C.S., Faria, S.H., 2013. High-resolution variations in size, number and arrangement of air bubbles in the EPICA DML (Antarctica) ice core. J. Glaciol. 59 (217), 972–980.

Fegyveresi, J.M., Alley, R.B., Spencer, M.K., Fitzpatrick, J.J., Steig, E.J., White, J.W.C., McConnell, J.R., Taylor, K.C., 2011. Late Holocene climate evolution at the WAIS Divide site, West Antarctica: bubble number-density estimates. J. Glaciol. 57 (204), 629–638.

Gow, A.J., 1968. Bubbles and bubble pressure in Antarctic glacier ice. CRREL Res. Rep. 249, 23.

Gow, A.J., 1969. On the rates of growth of grains and crystals in South Polar firn. J. Glaciol. 8 (53), 241–252.

Gow, A.J., Williamson, T., 1975. Gas inclusions in the Antarctic ice sheet and their glaciological significance. J. Geophys. Res. 80 (36), 5101–5108.

Hondoh, T., Shoji, H., Watanabe, O., Salamatin, A.N., Lipenkov, V.Y., 2002. Depth-age and temperature predictions at Dome Fuji station, East Antarctica. Ann. Glaciol. 35 (1), 384–390.

Jouzel, J., Alley, R.B., Cuffey, K.M., Dansgaard, W., Grootes, P., Hoffmann, G., Johnsen, S.J., Koster, R.D., Peel, D., Shuman, C.A., Stievenard, M., Stuiver, M., White, J., 1997. Validity of the temperature reconstruction from water isotopes in ice cores. J. Geophys. Res. 102 (C12), 26,471–26,487.

Jouzel, J., Masson-Delmotte, V., Cattani, O., Dreyfus, G., Falourd, S., Hoffmann, G., Minster, B., Nouet, J., Barnola, J.M., Chappellaz, J., Fischer, H., Gallet, J.C., Johnsen, S., Leuenberger, M., Loulergue, L., Luethi, D., Oerter, H., Parrenin, F., Raisbeck, G., Raynaud, D., Schilt, A., Schwander, J., Selmo, E., Souchez, R., Spahni, R., Stauffer, B., Steffensen, J.P., Stenni, B., Stocker, T.F., Tison, J.L., Werner, M., Wolff, E.W., 2007. Orbital and millennial Antarctic climate variability over the past 800,000 years. Science 317, 793, DOI: 10.1126/science.1141038.

Kawamura, K., Parrenin, F., Lisiecki, L., Uemura, R., Vimeux, F., Severinghaus, J.P., Hutterli, M.A., Nakazawa, T., Aoki, S., Jouzel, J., Raymo, M.E., Matsumoto, K., Nakata, H., Motoyama, H., Fujita, S., Goto-Azuma, K., Fujii, Y., Watanabe, O., 2007. Northern Hemisphere forcing of climatic cycles in Antarctica over the past 360,000 years. Nature 448, DOI: 10.1038/nature06015.

Kipfstuhl, S., Pauer, F., Kuhs, W.F., Shoji, H., 2001. Air bubbles and clathrate hydrates in the transition zone of the NGRIP deep ice core. Geophys. Res. Lett. 28 (4), 591–594.

Lipenkov, V.Ya., 2000. Air bubbles and air-hydrate crystals in the Vostok ice core, in: Hondoh, T. (Ed.). Physics of Ice Core Records. Sapporo, Hokkaido Univ. Press, pp. 243–282.

Lipenkov, V.Ya., Duval, P., Hondoh, T., Salamatin, A.N., Barkov, N.I., 1998. The climate signal in the air-bubble and air-hydrate records obtained from the deep Vostok ice core. EOS: Abstract 79 (45), Fall Meeting Suppl., F152.

Lipenkov, V.Ya., Ryskin, O.A., Barkov, N.I., 1999. Correlation between the number of air bubbles in ice and ice formation conditions. Materialy Glaciol. Issled. 86, 75–92.

Lipenkov, V.Ya., Salamatin, A.N., 2014. Steady-state size distribution of air bubbles in polar ice. Led i Sneg 54 (4), 20–31.

Lipenkov, V.Ya., Salamatin, A.N., Duval, P., 1997. Bubbly ice densification in ice sheets: II. Application. J. Glaciol. 43 (145), 397–407.

Maeno, N., Ebinuma, T., 1983. Pressure sintering of ice and its implication to the densification of snow at polar glaciers and ice sheets. J. Phys. Chem. 87 (21), 4103–4110.

Martinerie, P., Raynaud, D., Etheridge, D.M., Barnola, J.-M., Mazaudiera, D., 1992. Physical and climatic parameters which influence the air content in polar ice. Earth Planet. Sci. Lett. 112, 1–13.

Nichols, F.A., Mullins, W.W., 1965. Morphological changes of a surface of revolution due to capillarity- induced surface diffusion. J. Appl. Phys. 36 (6), 1826–1835, DOI: 10.1063/1.1714360.

Ohno, H., Lipenkov, V.Ya., Hondoh, T., 2004. Air bubble to clathrate hydrate transformation in polar ice sheets: A reconsideration based on the new data from Dome Fuji ice core. Geophys. Res. Lett. 31, L21401, DOI: 10.1029/2004GL021151.

Parrenin, F., Remy, F., Ritz, C., Siegert, M.J., Jouzel, J., 2004. New modeling of the Vostok ice flow line and implication for the glaciological chronology of the Vostok ice core. J. Geophys. Res., 109.

Pauer, F., Kipfstuhl, J., Kuhs, W.F., Shoji, H., 1999. Air clathrate crystals from the GRIP deep core: a number-, size-, and shape-distribution study. J. Glaciol. 45 (149), 22–30.

Petit, J.R., Jouzel, J., Raynaud, D., Barkov, N.I., Barnola, J-M., Basile, I., Bender, M., Chappellaz, J., Davis, M., Delaygue, G., Delmotte, M., Kotlyakov, V.M., Legrand, M., Lorius, C., Pépin, L., Ritz, C., Saltzman, E.S., Stievenard, M., 1999. Climate and atmospheric history of the past 420,000 years from the Vostok ice core, Antarctica. Nature 399 (6735), 429–436.

Robin, G. de Q., 1977. Ice cores and climatic change. Phil. Trans. Royal Soc. 280, 143–168.

Salamatin, A.N., Lipenkov, V.Ya., 2008. Simple relations for the close-off depth and age in dry snow densification. Ann. Glaciol. 49, 71–76.

Salamatin, A.N., Lipenkov, V.Ya., Barkov, N.I., Jouzel, J., Petit, J.R., Raynaud, D., 1998. Ice-core age dating and palaeothermometer calibration based on isotope and temperature profiles from deep boreholes at Vostok Station (East Antarctica). J. Geophys. Res. 103 (D8), 8963–8977.

Salamatin, A.N., Lipenkov, V.Ya., Barnola, J.-M., Hori, A., Duval, P., Hondoh, T., 2009. Snow/Firn densification in polar ice sheets, in: Hondoh, T. (Ed.). Physics of Ice Core Records. Sapporo, Hokkaido Univ. Press, 2, pp. 195–222.

Salamatin, A.N., Lipenkov, V.Ya., Duval, P., 1997. Bubbly ice densification in ice sheets: I. Theory. J. Glaciol. 43 (145), 387–396.

Saltykov, S.A., 1976. Stereometric Metallography. Nauka, Moscow, 248 pp. (in Russian)

Shieh, S.-Y., Evans, J.W., 1991. The stability of cylindrical voids and of cylinders subject to close-off by viscous flow or evaporation/condensation. J. Appl. Phys. 70 (6), 2968–2972.

Shoji, H., Langway, C.C. Jr., 1985. Mechanical properties of fresh ice core from Dye 3, Greenland, in: Langway, C.C. Jr., Oeschger, H., Dansgaard, W. (Eds). Greenland Ice Core: Geophysics, Geochemistry, and the Environment. Amer. Geophys. Union, Washington, DC, pp. 39–48. (Geophysical Monograph 33.)

Shreve, R.L., 1967. Migration of air bubbles, vapor figures, and brine pockets in ice under a temperature gradient. J. Geophys. Res. 72 (16), 4093–4100.

Shumskiy, P.A., 1955. Fundamentals of Structural Ice Science. AN SSSR, Moscow, 492 pp. (in Russian)

Stauffer, B., Schwander, J., Oeschger, H., 1985. Enclose-off of air during metamorphosis of dry firn to ice. Ann. Glaciol. 6, 108–112.

Stehle, N.S., 1967. Migration of bubbles in ice under a temperature gradient, in: Ôura, H. (Ed.). Physics of Snow and Ice: International Conference on Low Temperature science, 1966: Proc. 1, Pt. 1. Sapporo, Japan, Instit. Low Temperature Sci., Hokkaido Univ., pp. 219–232.

Thorsteinsson, T., 1996. Textures and fabrics in the GRIP ice core, in relation to climate history and ice deformation. Rep. Polar Res. 205, 1–145.

Tsyganova, E.A., Salamatin, A.N., 2004. Non-steady-state temperature field simulation along the ice flow line "Ridge B–Vostok Station", East Antarctica. Materialy Glaciol. Issled. 97, 57–70.

Ueltzhöffer, K.J., Bendel, V., Freitag, J., Kipfstuhl, S., Wagenbach, D., Faria, S.H., Garbe, C.S., 2010. Distribution of air bubbles in the EDML and EDC (Antarctica) ice cores, using a new method of automatic image analysis. J. Glaciol. 56 (196), 339–348.

Underwood, E.E., 1970. Quantitative steorology. Reading. Addison-Weslet Publ. Co., MA, USA, 358 pp.

Watanabe, O., Jouzel, J., Johnsen, S., Parrenin, F., Shoji, H., Yoshida, N., 2003. Homogeneous climate variability across East Antarctica over the past three glacial cycles. Nature 422 (6931), 509–512.

Weertman, J., 1968. Bubble coalescence in ice as a tool for the study of its deformation history. CREEL Res. Rep., No. 251, 17 pp.

Received March 7, 2017